DOI: 10.71762/rzhv-y041

Research Paper

Evaluation of Hydroforming Parameters for Motorcycle Exhaust Pipe Production Using FEM Simulation

Mohammad Sajjad Mahdieh*[1], Farshad Nazari[1], Laith Jawad[1]
[1]Department of Mechanical Engineering, Shahid Chamran University of Ahvaz, Ahvaz, Iran
*Email of Corresponding Author: s.mahdieh@scu.ac.ir
Received: February 8, 2025; Accepted: April 18, 2025

Abstract
By utilizing the hydroforming technique, parts with enhanced fatigue strength can be produced without the need for welding seams. Additionally, in the automotive sector, the production of complex cylindrical components from metal pipes has gained attention, particularly for improving the strength-to-weight ratio and reducing vehicle fuel consumption. As a result, automobile manufacturers have increasingly focused on this method. Understanding the key factors influencing the successful execution of this process is essential for achieving high-quality products, optimal geometry, improved efficiency, and cost reduction. To examine material behavior during hydroforming and to avoid significant material loss, simulation procedures are crucial. This study investigates the manufacturing of motorcycle exhaust pipes through the hydroforming process, using FEM simulation (ABAQUS software), and calculates the optimal die geometry, required press force, and fluid pressure. Simulation results from ABAQUS demonstrate that the part is fully formed with an internal fluid pressure of 8.5 MPa and an axial load of 1120 kN.

Keywords
Metal Forming, Hydroforming Process, ABAQUS, Automotive Industry, FEM Simulation

1. Introduction

In recent decades, hydroforming has emerged as one of the most widely adopted methods for shaping industrial components with continuous, integrated sections. A significant number of industrial parts, particularly in the automotive industry, are produced through this process. These components typically feature complex geometries, a single-piece structure, high fatigue strength, and reduced weight. Moreover, in mass production, since the hydroforming process involves a single-stage production, it enhances the production rate and significantly lowers manufacturing costs. As a result, investigating the key factors that contribute to the proper execution of this process is essential for achieving high-quality products with optimal geometry. Additionally, following the hydroforming process, finishing operations such as grinding, vibratory finishing, burnishing, and barrel finishing are typically unnecessary [1-4]. Tube hydroforming is employed to shape tubular components, such as brackets for bicycle frames or pipe fittings. Both axial force and internal pressure are applied to the tube, generating compressive stress in one direction. This results in the deformation of the tube elements with reduced thinning and risk of tearing (Figure 1). By utilizing specially designed forming machines, this process allows for the production of a high volume of parts at a relatively low cost [5-13]. To analyze material behavior during the hydroforming process, both the theoretical formulations for modeling and the simulation procedures must be taken into account.

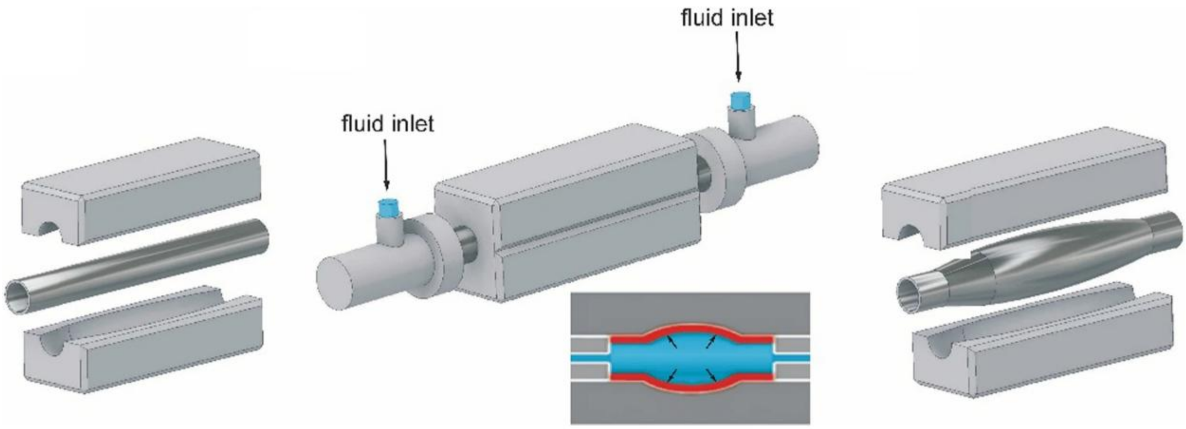

Figure 1. Schematic of tube hydroforming [14]

In recent years, substantial research has been conducted to simulate and optimize forming processes, such as hydroforming, to produce flawless parts [15-17]. At the mass production scale, the hydroforming process proves to be more efficient and cost-effective compared to other manufacturing methods, such as machining, non-traditional machining, and sheet metal processes [18-26]. Snafi [27-29], to predict rupture, analyzed the hydroforming model of the pipe and examined its plastic deformation. He used the local throat criterion to predict rupture. Neffusi et al. [30] used the Swift criterion to predict a diffuse throat in sheet forming and pipe hydroforming. They studied buckling and choking simultaneously. They showed analytically and numerically that the strain limit for buckling is less than the strain limit for the throat. Kim et al. [31] performed finite element analysis to predict rupture in the pipe hydroforming process and used diffusion plastic instability to numerically predict the forming limit. For anisotropic pipes, a plastic potential developmental solution was considered based on the quadratic Hill criterion. Through this theory, they investigated the effects of anisotropy on the strain limit and rupture pressure. In addition, Bomaiza et al. [32] studied the plastic instability of elastoplastic tubes relative to internal pressure and proposed a new diffusion measurement criterion that included geometric effects. In another research, Sorenin et al. [33] simulated the hydroforming process for both T and Y-shaped pipes and investigated the instability of the plastic using a defective model. In the same year, Butcher et al. [34] investigated a high-carbon steel pipe using a defect model in the hydroforming process and compared the results with laboratory results. In 2010, Craps et al. [35] performed finite element analysis using a time-dependent solution variable for the T-shaped copper pipe hydroforming process and a criterion for changing various process parameters (pressure and velocity paths) relative to the final product. Moreover, Li et al. [36] were able to form various parts with high expansion ratios and variable cross sections along the pipe, as well as with different materials such as aluminum alloy and stainless steel, using the pipe hydroforming process, by applying high internal pressure. The key point of their research is to create useful initial wrinkles in the tube to achieve the desired final shape. Hashemi et al. [37] predicted the bursting of the pipe in the hydroforming process, when loaded with axial feeding, analytically and based on the instability of the plastic. In addition, in 2016, Desu et al. [38] worked on the mechanical properties of Austenitic Stainless Steel grade 304L and 316L at high temperatures. Gheisary et al. in 2010 established a basic understanding of the double bulge tube hydroforming process of stainless steel deep-drawn cups. Their method was briefly reviewed by carrying out experimental tests and Finite element analysis [39]. Hwang et al. used the finite element method to explore the plastic flow pattern of a circular tube that is hydraulically expanded or crushed into a rectangular cross-section. The tubes used in the crushing process have larger diameters and are thinner than the tubes used in the hydraulic expansion test. The loading path and the forming procedures during the crushing process are discussed [40,41]. Kashani and Khorsandi, in separate research, worked on the simulation of tube hydroforming of unequal T joints with the finite element method. They used ABAQUS in their study, and they investigated the effects of the coefficient of friction, strain hardening exponent, and fillet radius on the parameters and thickness distribution of the process [42,43]. Choi et al. made a comparison of an implicit and an explicit finite-element method which is widely used for the hydroforming process [44]. Bakhshi et al. studied the pulsating hydroforming of a tube with a box die which was simulated by the finite element method to examine the effect of pulsating pressure on the improvement of formability [45]. Mohammadalizade et al. investigated the effects of internal pressure and axial feeding paths to improve the thickness distribution of stepped cylindrical tubes [46].

This study investigates the feasibility of manufacturing a motorcycle exhaust pipe (Figure 2) using the hydroforming process through FEM simulation. To determine the hydroforming parameters, such as fluid pressure, material thickness reduction, and maximum stress and strain, the process is simulated using ABAQUS software. The simulations then provide insights into key factors, including maximum tensile stress, thickness reduction, formability, and the potential for cracks and rupture.

Figure 2. Case study of this paper: motorcycle exhaust pipe

2. Materials and methods

This study explores the feasibility of manufacturing a motorcycle exhaust pipe using the hydroforming process through FEM simulation. To create a 3D model of the die, the dimensions of the part were first required. As a result, the motorcycle exhaust pipe was digitized using a 3D scanner, and the cloud points were extracted. Subsequently, the 3D model was generated using the Shape Design module of Catia software. The initial part and the hydroforming die were then designed and modeled in Catia, as shown in Figures 3 and 4, respectively. The thickness of the initial part is assumed to be 0.5mm.

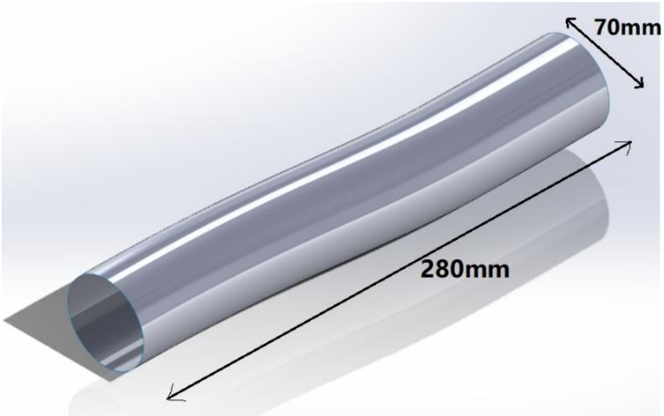

Figure 3. Model of the initial part

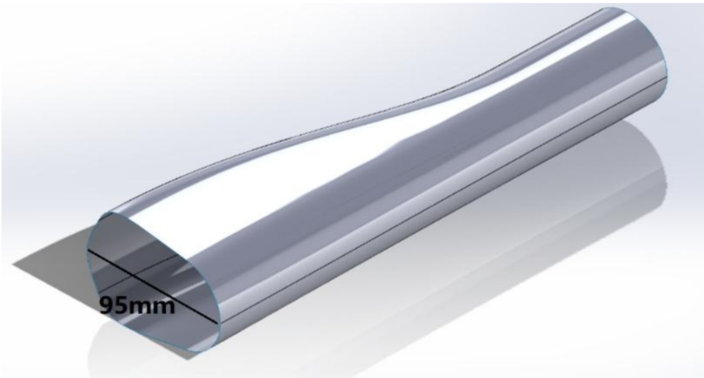

Figure 4. The 3D model of the final part (die)

Due to the exposure of the motorcycle exhaust pipe to high temperatures, humidity, dust, and other contaminants, corrosion is a common issue on its surface. As a result, a corrosion-resistant material, such as stainless steel, is ideal for this application. In this study, 304 stainless steel, a widely used alloy for such purposes, is selected. For the simulation of the metal forming process, it is essential to consider the plastic or strain-hardening region of the material properties. To achieve this, the Johnson-Cook plasticity equation or tabular stress versus equivalent plastic strain data can be utilized. In this research, tabular data is used for its simplicity and availability. The mechanical properties of the 304 stainless steel, as used in the Property module of ABAQUS, are listed in Table 1, and its chemical composition is provided in Table 2. The stress-strain data for the plastic region are presented in Table 3, and the σ-ε curves for 304 stainless steel at various temperatures are shown in Figure 5.

Table 1. The mechanical properties of 304 stainless steel [47]

Type	E% in 50mm	YS(Mpa)	UTS (MPa)	Hardness (Rockwell B)
304	45%	205	550	92

Table 2. The chemical composition of 304 stainless steel [47]

Element	%Wt
C	0.0 - 0.07
Mn	0.0 - 2.0
Si	0.0 - 1.00
P	0.0 - 0.05
S	0.0 - 0.03
Cr	17.50 - 19.50
Ni	8.00 - 10.50
Fe	Balance

Table 3: plastic region stress-strain data [48]

Yield stress (MPa)	Equivalent plastic strain
91.294	0
121.290	0.00097685
161.290	0.004812
201.290	0.01411
241.29	0.032819
281.290	0.066236
321.290	0.12114
361.290	0.20588
401.290	0.33054
441.290	0.50696
481.290	0.7489
521.290	1.0721

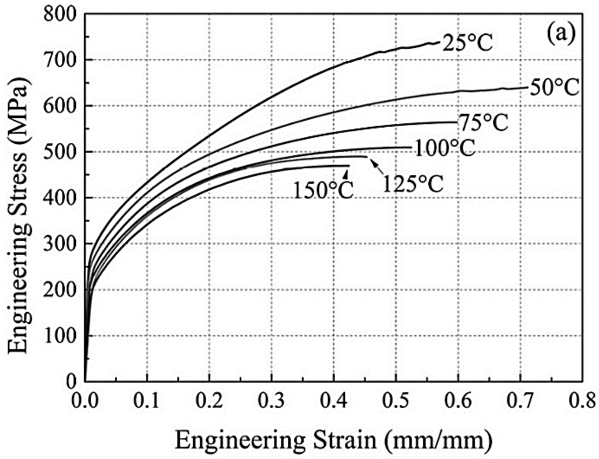

Figure 5. σ-ε curves of 304 stainless steel [48]

In this study, the simulations are performed in ABAQUS software version 2022. The initial part imported into the Part module is 3D and formable, and on the other hand, the die is solid and rigid. The assembly of the die and initial part is performed in the Assembly module, which is shown in Figure 6.

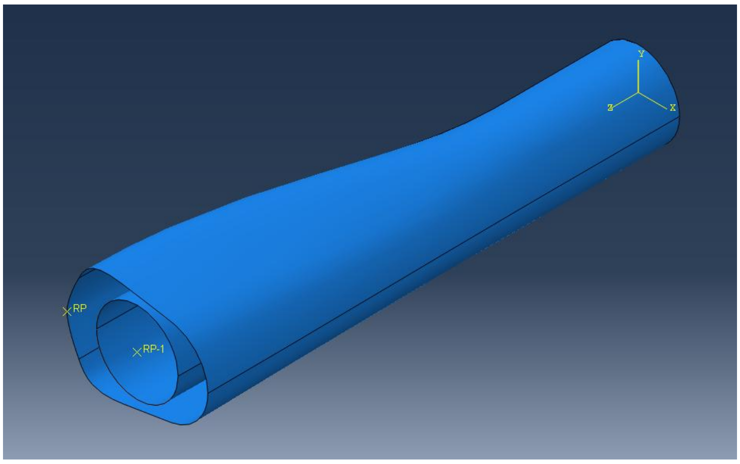

Figure 6. Assembly of the die and initial part in the Assembly module

A lubricating oil film with a friction coefficient of 0.1 is applied to the simulation. In the Properties module of ABAQUS, the material properties such as Young's modulus (210 GPa), Poisson's ratio (0.3), and density (7800 kg/m^3) are entered. The stress-strain curve of metallic materials typically exhibits three distinct regions. The first region is the elastic region, where a linear relationship between stress and strain is observed. In the second region, strain hardening occurs, and the stress increases significantly with strain. The third region is necking, where damage begins to develop. The relationship between stress and strain in the plastic behavior of the material is selected based on prior studies and imported into ABAQUS.

The material is modeled as a shell with a thickness of 0.5mm. The Explicit Dynamic solver is chosen in the Step module to solve the problem and carry out the simulation. In the Load module, an internal pressure of 8.5 MPa is applied to the internal surface of the part. Additionally, during the hydroforming process simulation, tangential pressure is applied because the pressure magnitude is assumed to be the same in all directions. Tangential pressure is applied in the Load module using the surface traction option. This value was determined through a trial-and-error method. The objective was to fully form the part and fill the die, which is the criterion for the appropriate pressure. The axial load applied to both ends of the part is 1120 kN, which was also determined through trial and error.

In the Mesh module, a mesh size of 0.2 mm and the standard shell (S4R) mesh type are selected, given the thin wall of the part. Figure 7 illustrates the meshed components.

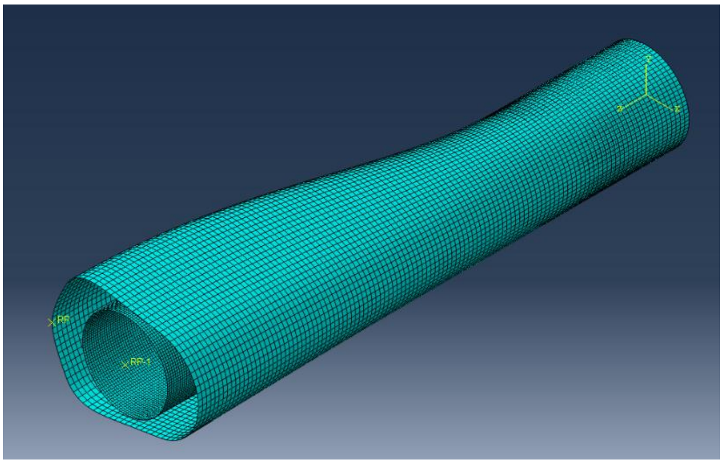

Figure 7. Meshed parts

3. Results and Discussion

This section investigates the feasibility of manufacturing the motorcycle exhaust pipe via the hydroforming process through FEM simulation. The hydroforming parameters, including fluid pressure, material thickness reduction, and maximum stress and strain, were determined through ABAQUS simulations. The results on maximum tensile stress, thickness reduction, formability, and the occurrence of cracks and rupture are presented below.

3.1 Internal Pressure and Axial Load

The internal pressure for the hydroforming process was determined using a trial-and-error approach, a common method in cases where precise experimental data or analytical models are unavailable. The pressure was incrementally increased in small steps, allowing the tube to gradually expand and fill the die. During this process, it was observed that higher internal pressures lead to an increase in forming efficiency, as they ensure that the material flows more easily into the die, filling all sections and achieving the desired shape. However, excessively high pressure significantly increases the process cost due to higher energy requirements and increased wear on the tooling, which can also lead to potential material damage or failure. On the other hand, insufficient internal pressure results in incomplete forming, where parts of the tube may not fill the die fully, leading to defects such as wrinkles, incomplete shapes, or inconsistent material distribution. By carefully balancing these factors, the simulation indicated that an optimal internal pressure of 8.5MPa achieved the best combination of material flow, geometric accuracy, and process efficiency. Furthermore, the required axial load to form the final geometry of the motorcycle exhaust pipe was determined to be 1120kN, which ensures that the material is adequately constrained and deformed in the axial direction to complete the shaping process while maintaining structural integrity and avoiding unwanted deformation such as necking or fracture.

3.2 Maximum Stress

Figure 8 illustrates the various stages of tube forming, from the initial step to the final shape. The tube progressively takes shape as internal pressure is applied. As shown in the figure, the tube is fully formed and fills the die, with no rupture or wrinkles appearing in the final part. This outcome indicates that the selected forming parameters, including internal pressure and the coefficient of friction, were appropriate.

The maximum and minimum stresses induced in the tube are presented in Figure 9. As shown, the maximum stress, approximately 378 MPa, occurs at the front of the nose of the tube, where the greatest deformation takes place. In contrast, the minimum stress of 3 MPa occurs at the bottom of the tube, which undergoes less deformation.

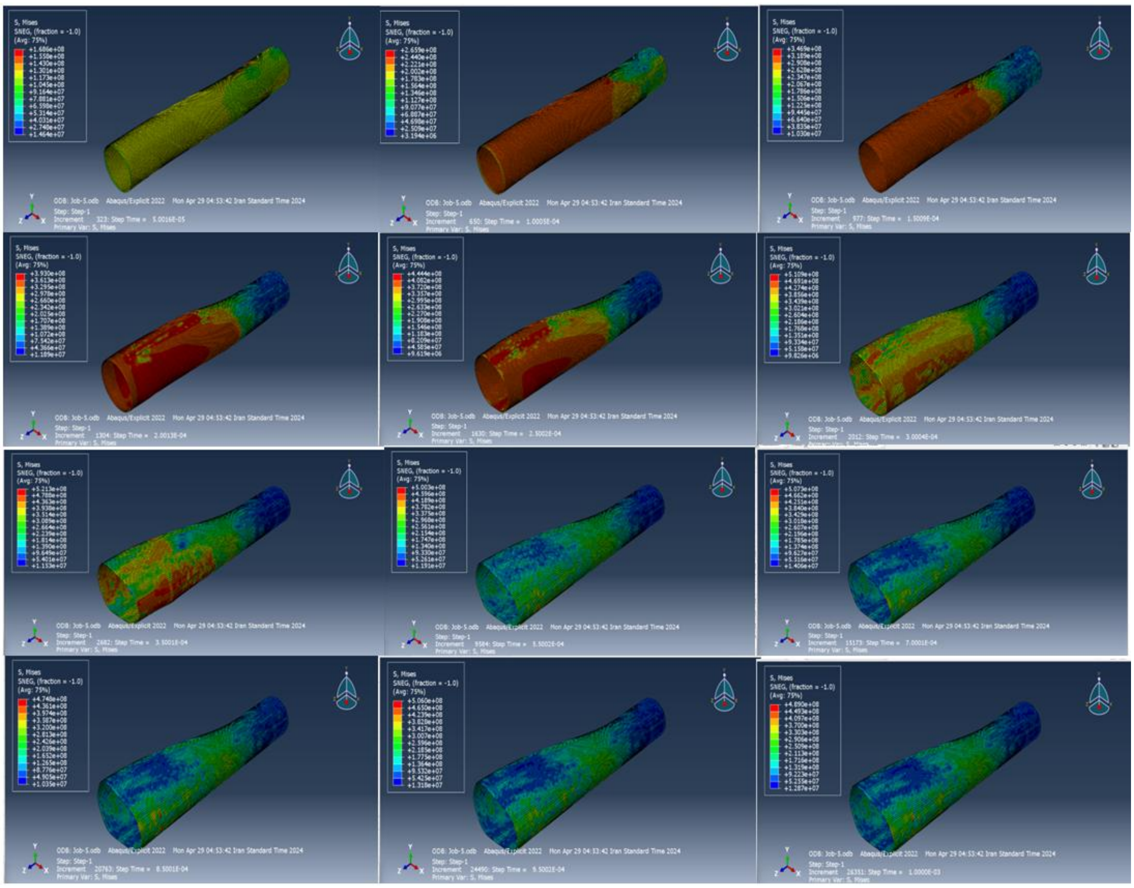

Figure 8. The simulation steps and stresses in each step

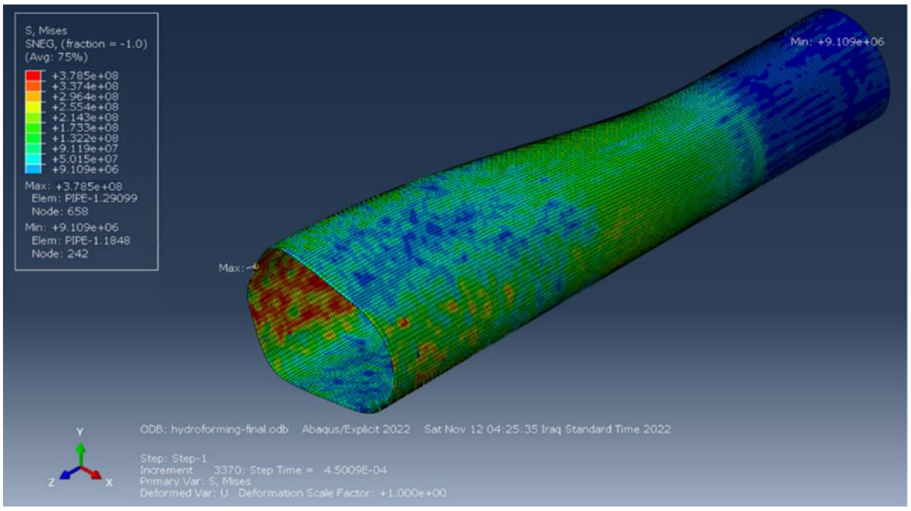

Figure 9. The Maximum and minimum stresses

The stress in the die equals 237 MPa (Figure 10). This stress is lower than the yield stress of the die (237 MPa) because the internal pressure is applied to the internal surface of the part, and the die only experiences pressure from the formed part during the final stage of the forming process.

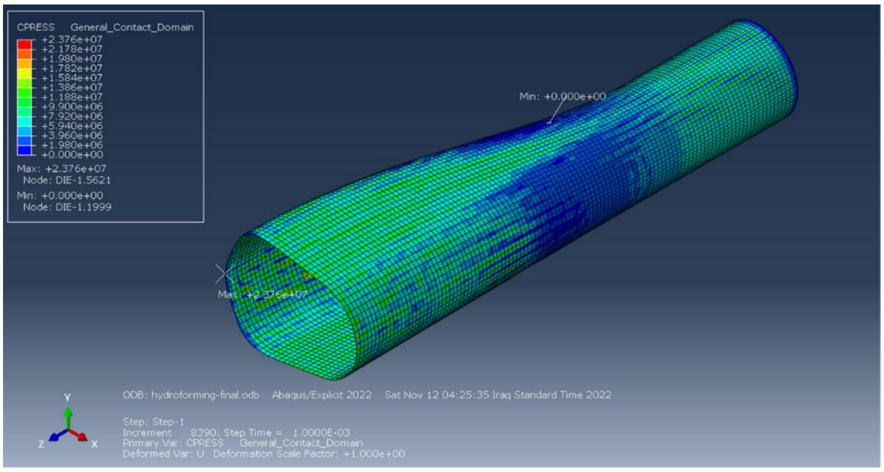

Figure 10. The Maximum stress induced in the die

3.3 Maximum strain

According to Figure 11, the maximum strain appears near the nose of the part, and it equals 0.8215.

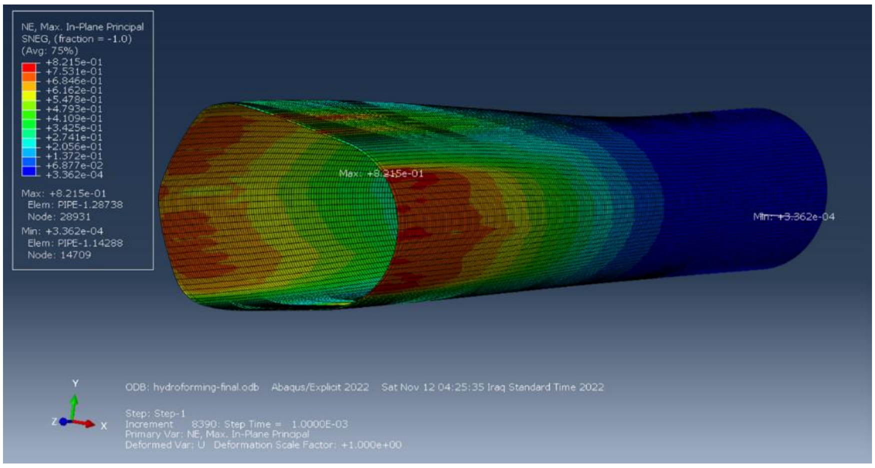

Figure 11. The Maximum strain

3.4 Reduction in thickness

The reduction in shell thickness plays a crucial role in influencing various aspects of the forming process. Excessive thinning can lead to material rupture, whereas insufficient thickness reduction raises concerns about whether the initial thickness is appropriate or overly conservative. In this study, the raw tube initially had a thickness of 0.5 mm, which decreased to 0.29 mm at the critical point after the hydroforming process. This reduction is within an acceptable range, ensuring both structural integrity and manufacturability. The elongation at the crucial point was measured at 41%, which remains below the maximum allowable elongation (45%) for a single-step forming process. This indicates that the forming operation was successfully conducted without any rupture, confirming the reliability and efficiency of the applied parameters. The thickness of the final part is shown in Figure 12.

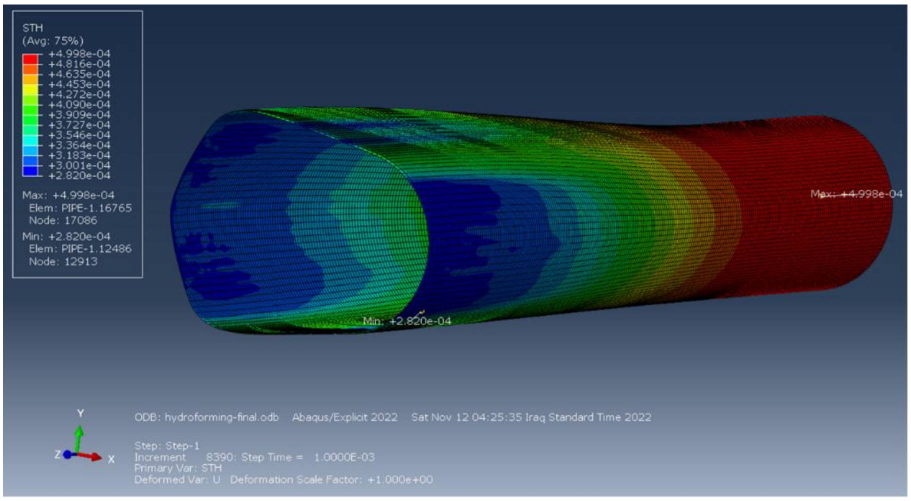

Figure 12. Thickness of the final part

The simulation results indicate that the forming process was executed flawlessly, with the sheet metal filling the die and the edges being perfectly formed. Figure 13 shows the convergence of the stress result as the number of mesh elements increases. According to the figure, at a point on the part, with

15000 mesh elements (mesh size of 0.4 mm), the stress is 205 MPa. As the mesh elements are increased to 30000 (mesh size of 0.2 mm), the result converges to 375 MPa.

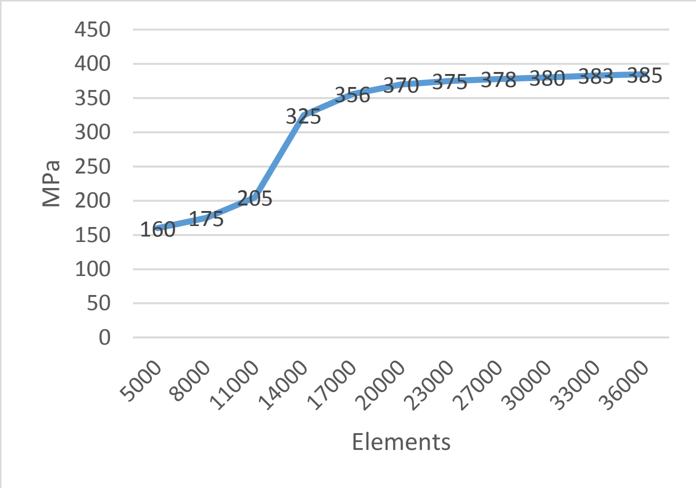

Figure 13. Convergence of results (stress) by increasing the number of mesh

3.5 Verification

Due to the absence of direct experimental data for the motorcycle exhaust pipe manufacturing process, the results obtained from the FEM simulation were compared with similar studies on hydroforming of automotive components. The simulation parameters, including material properties and boundary conditions, were carefully selected based on established data from comparable metal-forming processes, ensuring the model's accuracy. Additionally, a mesh refinement study was conducted, where the simulation results showed convergence with the reduction in mesh size, further validating the model's precision. Although the simulations provide valuable insights into the hydroforming process, experimental validation will be necessary to fully confirm the results. Therefore, the current study serves as an initial step, with future physical prototype testing planned to validate the findings and refine the model.

However, in Reference [13], a detailed investigation was conducted on the manufacturing of an automobile exhaust pipe, as depicted in Figure 14. The parameters and findings of that study are summarized in Table 4 and compared with the results of the present work. According to study [13], the thickness reduction in the exhaust pipe was approximately 18%, and the maximum stress recorded was 290 MPa. In contrast, the present study demonstrates a thickness reduction of 41% and a maximum stress of 378 MPa. While a direct comparison between these parameters is challenging due to differences in process conditions and dimensions, the observed trends provide a reasonable basis for validating the results of the current study.

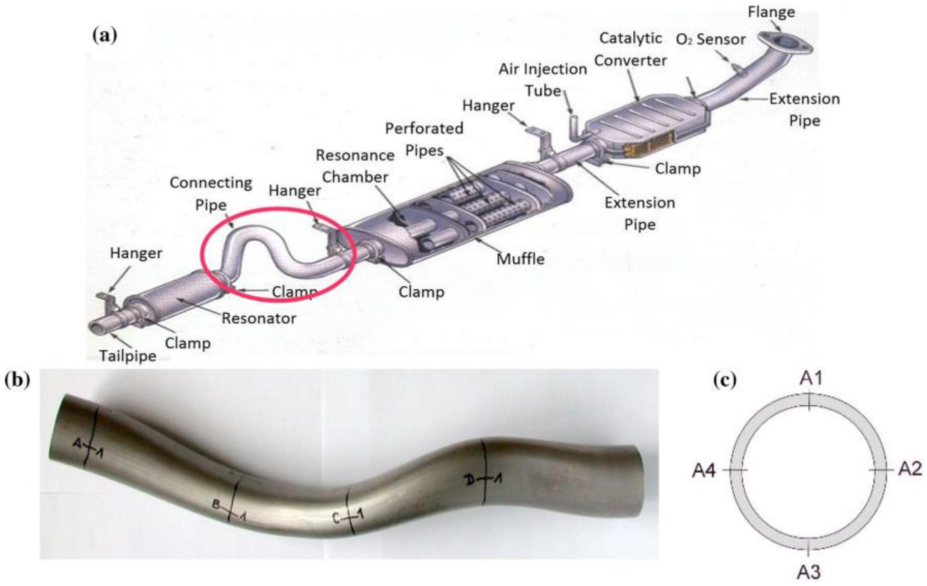

Figure 14. Case study according to the study [13]

Table 4. Comparison of the parameters of study [13] and the present study

parameters	Ref [13]	present study
Material	Stainless steel 304	Stainless steel 304
Initial thickness	1.2mm	0.5mm
Temperature	25ºC	25ºC
Max stress	290	378
Max thickness reduction	18%	41%
Fluid pressure	18MPa	8.5MPa
Axial load	Not indicated	1120kN

4. Conclusions

In this study, the feasibility of manufacturing the motorcycle exhaust pipe through the hydroforming process was explored via FEM simulation. The key results are summarized as follows:

- The internal pressure was determined using the trial-and-error method. The pressure was increased until the tube was fully formed and the die was filled. The final internal pressure obtained from the simulation is 8.5 MPa. Additionally, the axial load required to form the final geometry of the pipe was found to be 1120 kN.

- The maximum stress, approximately 378 MPa, occurs at the front of the nose of the tube due to the highest deformation in this area. In contrast, the minimum stress, equal to 3 MPa, occurs at the bottom of the tube, where deformation is minimal.
- The maximum strain is observed near the nose of the part, with a value of 0.8215.
- The raw tube initially had a thickness of 0.5 mm, which decreased to 0.29 mm at the critical point after the hydroforming process. This reduction is within an acceptable range, ensuring both structural integrity and manufacturability. The elongation at the critical point was

measured at 41%, which remains below the maximum allowable elongation (45%) for a single-step forming process.

5. Acknowledgment

We are grateful to the Research Council of Shahid Chamran University of Ahvaz for financial support (SCU.EM1404.39184).

6. References

[1] Mahdieh, M.S., Rafati, E. and Kargar Sichani, S. 2013. Investigation of variance of roller burnishing parameters on surface quality by taguchi approach. ADMT Journal. 6(3).

[2] Saraeian, P., Gholami, M., Behagh, A., Behagh, O., Javadinejad, H.R. and Mahdieh, M. 2016. Influence of vibratory finishing process by incorporating abrasive ceramics and glassy materials on surface roughness of ck45 steel. ADMT Journal. 9(4): 1-6.

[3] Vakili Sohrforozani, A., Farahnakian, M., Mahdieh, M.S., Behagh, A.M. and Behagh, O. 2019. A study of abrasive media effect on deburring in barrel finishing process. Journal of Modern Processes in Manufacturing and Production. 8(3): 27-39.

[4] Vakili Sohrforozani, A., Farahnakian, M., Mahdieh, M.S., Behagh, A.M. and Behagh, O. 2020. Effects of abrasive media on surface roughness in barrel finishing process. ADMT Journal. 13(3): 75-82.

[5] Alaswad, A., Benyounis, K. and Olabi, A. 2012. Tube hydroforming process: A reference guide. Materials & Design. 33: 328-339. doi: 10.1016/j.matdes.2011.07.052.

[6] Ahmetoglu, M. and Altan, T. 2000. Tube hydroforming: State-of-the-art and future trends. Journal of Materials Processing Technology. 98(1): 25-33. doi: 10.1016/S0924-0136(99)00302-7.

[7] Ahmetoglu, M., Sutter, K., Li, X. and Altan, T. 2000. Tube hydroforming: Current research, applications and need for training. Journal of materials processing technology. 98(2): 224-231. doi: 10.1016/S0924-0136(99)00203-4.

[8] Siegert, K., Häussermann, M., Lösch, B. and Rieger, R. 2000. Recent developments in hydroforming technology. Journal of Materials Processing Technology. 98(2): 251-258. doi: 10.1016/S0924-0136(99)00206-X.

[9] Koç, M. and Altan, T. 2001. An overall review of the tube hydroforming (thf) technology. Journal of Materials Processing Technology. 108(3): 384-393. doi: 10.1016/S0924-0136(00)00830-X.

[10] Bell, C., Corney, J. and Zuelli, N. 2020. A state of the art review of hydroforming technology. International Journal of Material Forming. 13(5): 789-828. doi:10.1007/s12289-019-01507-1.

[11] Lee, M.-G., Korkolis, Y.P. and Kim, J.H. 2015. Recent developments in hydroforming technology. Proceedings of the Institution of Mechanical Engineers, Part B: Journal of Engineering Manufacture. 229(4): 572-596. doi: 10.1177/095440541454.

[12] Mahdieh, M.S. and Esteki, M.R. 2022. Feasibility investigation of hydroforming of dental drill body by fem simulation. Journal of Modern Processes in Manufacturing and Production. 11(2): 71-83. dor: 20.1001.1.27170314.2022.11.2.7.5

[13] Cheng, L., Guo, H., Sun, L., Yang, C., Sun, F. and Li, J. 2024. Real-time simulation of tube hydroforming by integrating finite-element method and machine learning. Journal of Manufacturing and Materials Processing. 8(4): 175. doi: 10.3390/jmmp8040175.

[14] Kucharska, B. and Moraczyński, O. 2020. Exhaust system piping made by hydroforming: Relations between stresses, microstructure, mechanical properties and surface. Archives of Civil and Mechanical Engineering. 20(4): 141. doi:10.1007/s43452-020-00142-x.

[15] Liu, C., Abd El-Aty, A., Lee, M.-G., Hou, Y., Xu, Y., Hu, S., Cheng, C., Tao, J. and Guo, X. 2023. Predicting the forming limits in the tube hydroforming process by coupling the cyclic plasticity model with ductile fracture criteria. Journal of Materials Research and Technology. 26: 109-120. doi: 10.1016/j.jmrt.2023.07.177.

[16] Liu, X.J., Zou, Z.L., Zhou, Y.Y. and Li, C. 2024. Study on hydroforming of aluminum alloy thin-wall curved parts based on upper layer sheet and numerical simulation. The International Journal of Advanced Manufacturing Technology. 132(11): 5733-5752.doi: 10.1007/s00170-024-13581-0.

[17] Marlapalle, B.G. and Hingole, R.S. 2021. Predictions of formability parameters in tube hydroforming process. SN Applied Sciences. 3(6): 606. doi:10.1007/s42452-021-04533-4.

[18] Mahdieh, M.S. 2020. The surface integrity of ultra-fine grain steel, electrical discharge machined using iso-pulse and resistance–capacitance-type generator. Proceedings of the Institution of Mechanical Engineers, Part L: Journal of Materials: Design and Applications. 234(4): 564-573. doi: 10.1177/1464420720902782.

[19] Mahdieh, M.S. 2020. Recast layer and heat-affected zone structure of ultra-fined grained low-carbon steel machined by electrical discharge machining. Proceedings of the Institution of Mechanical Engineers, Part B: Journal of Engineering Manufacture. 234(5):933-944. doi: 10.1177/0954405419889202.

[20] Mahdieh, M.S. and Mahdavinejad, R. 2016. Comparative study on electrical discharge machining of ultrafine-grain al, cu, and steel. Metallurgical and Materials Transactions A. 47(12): 6237-6247. doi: 10.1007/s11661-016-3741-y.

[21] Mahdieh, M.S. and Zare-Reisabadi, S. 2019. Effects of electro-discharge machining process on ultra-fined grain copper. Proceedings of the Institution of Mechanical Engineers, Part C: Journal of Mechanical Engineering Science. 233(15): 5341-5349. doi:10.1177/0954406219844802.

[22] Mahdieh, M.S. and Mahdavinejad, R.A. 2017. A study of stored energy in ultra-fined grained aluminum machined by electrical discharge machining. Proceedings of the Institution of Mechanical Engineers, Part C: Journal of Mechanical Engineering Science. 231(23): 4470-4478. doi: 10.1177/0954406216666872.

[23] Mahdieh, M.S. and Mahdavinejad, R. 2018. Recast layer and micro-cracks in electrical discharge machining of ultra-fine-grained aluminum. Proceedings of the Institution of Mechanical Engineers, Part B: Journal of Engineering Manufacture. 232(3): 428-437. doi: 10.1177/0954405416641326.

[24] Feng, Y., Chen, G., Geng, S. and Shan, J. 2025. Cross scale numerical simulation and experimental study on hydroforming of double-layer y-shaped tube. Modelling and Simulation in Materials Science and Engineering. 33(3): 035006. doi: 10.1088/1361-651X/adbc05/meta.

[25] Raut, S.V., Ramesh, A., Arun, A. and Sumesh, C. 2021. Finite element analysis and optimization of tube hydroforming process. Materials Today: Proceedings. 46: 5008-5016. doi: 10.1016/j.matpr.2020.10.394.

[26] Zhu, Q.-q., Huang, S., Wang, D.-x., Li, J.-p., Hua, F.-a. and Yang, P. 2022. Numerical simulation and experimental study of warm hydro-forming of magnesium alloy sheet. Journal of Manufacturing Processes. 80: 43-53. doi: 10.1016/j.jmapro.2022.05.054.

[27] Asnafi, N. 1999. Analytical modelling of tube hydroforming. Thin-walled structures. 34(4): 295-330. doi: 10.1016/S0263-8231(99)00018-X.

[28] Asnafi, N. and Skogsgårdh, A. 2000. Theoretical and experimental analysis of stroke-controlled tube hydroforming. Materials Science and Engineering: A. 279(1-2): 95-110. doi: 10.1016/S0921-5093(99)00646-2.

[29] Mahdieh, M.S. and Monjezi, A. 2022. Investigation of an innovative cleaning method for the vertical oil storage tank by fem simulation. Iranian Journal of Materials Forming. doi: 10.22099/ijmf.2022.43842.1229.

[30] Nefussi, G. and Combescure, A. 2002. Coupled buckling and plastic instability for tube hydroforming. International Journal of Mechanical Sciences. 44(5): 899-914. doi: 10.1016/S0020-7403(02)00031-0.

[31] Kim, J., Kim, S.-W., Song, W.-J. and Kang, B.-S. 2004. Analytical approach to bursting in tube hydroforming using diffuse plastic instability. International journal of mechanical sciences. 46(10): 1535-1547. doi: 10.1016/j.ijmecsci.2004.09.001.

[32] Boumaiza, S., Cordebois, J.-P., Brunet, M. and Nefussi, G. 2006. Analytical and numerical study on plastic instabilities for axisymmetric tube bulging. International journal of mechanical sciences. 48(6): 674-682. doi: 10.1016/j.ijmecsci.2005.12.012.

[33] Sornin, D., Fayolle, S., Bouchard, P.-O. and Massoni, E. 2009. Plastic instabilities analysis during t-shaped tubes hydro-forming process. International Journal of Material Forming. 2(2): 131-144. doi: 10.1007/s12289-009-0399-7.

[34] Butcher, C., Chen, Z., Bardelcik, A. and Worswick, M. 2009. Damage-based finite-element modeling of tube hydroforming. International Journal of Fracture. 155(1): 55-65. doi: 10.1007/s10704-009-9323-x.

[35] Crapps, J., Marin, E., Horstemeyer, M., Yassar, R. and Wang, P. 2010. Internal state variable plasticity-damage modeling of the copper tee-shaped tube hydroforming process. Journal of Materials Processing Technology. 210(13): 1726-1737. doi: 10.1016/j.jmatprotec.2010.06.003.

[36] Li, H., Wang, X., Yuan, S., Miao, Q. and Wang, Z. 2004. Typical stress states of tube hydroforming and their distribution on the yield ellipse. Journal of Materials Processing Technology. 151(1-3): 345-349. doi: 10.1016/j.jmatprotec.2004.04.085.

[37] Afshar, A., Hashemi, R., Madoliat, R., Rahmatabadi, D. and Hadiyan, B. 2017. Numerical and experimental study of bursting prediction in tube hydroforming of al 7020-t6. Mechanics & Industry. 18(4): 411. doi: 10.1051/meca/2017019.

[38] Desu, R.K., Krishnamurthy, H.N., Balu, A., Gupta, A.K. and Singh, S.K. 2016. Mechanical properties of austenitic stainless steel 304l and 316l at elevated temperatures. Journal of Materials Research and Technology. 5(1): 13-20. doi: 10.1016/j.jmrt.2015.04.001.

[39] Gheisary, M. and Djavanroodi, F. 2010. Experimental and numerical investigation of double bulge tube hydroforming. Modares Mechanical Engineering. 10(3): 1-9. dor: 20.1001.1.10275940.1389.10.3.8.3.

[40] Hwang, Y. M. and Altan, T. 2003. Finite element analysis of tube hydroforming processes in a rectangular die. Finite Elements in Analysis and Design. 39(11): 1071-1082. doi: 10.1016/S0168-874X(02)00157-9.

[41] Hwang, Y.-M. and Lin, Y.-K. 2002. Analysis and finite element simulation of the tube bulge hydroforming process. Journal of materials processing technology. 125: 821-825. doi: 10.1016/S0924-0136(02)00381-3.

[42] Zadeh, H.K. and Mashhadi, M.M. 2006. Finite element simulation and experiment in tube hydroforming of unequal t shapes. Journal of Materials Processing Technology. 177(1-3): 684-687. doi: 10.1016/j.jmatprotec.2006.04.056.

[43] Khorsandi, A. and Loh-Mousavi, M. 2010. Numerical investigations on the effect of pulsating pressure on improvement of formability in hydroforming of bent tube by fem. Journal of Simulation and Analysis of Novel Technologies in Mechanical Engineering. 3(1): 11-20.

[44] Choi, H.-H., Hwang, S.-M., Kang, Y., Kim, J. and Kang, B. 2002. Comparison of implicit and explicit finite-element methods for the hydroforming process of an automobile lower arm. The International Journal of Advanced Manufacturing Technology. 20(6): 407-413. doi: 10.1007/s001700200170.

[45] Bakhshi-Jooybari, M.L.-M.M. and Hosseinipour, K.M.M.F.S. Experimental study and numerical study of pulsating hydroforming of tube in box-shaped die.

[46] Mohammadalizade, F., Gorji, A., Bakhshi, M. and Elyasi, M. 2016. Reforming internal pressure and axial feeding loading paths in hydroforming process of cylindrical stepped tube in order to improve the thickness distribution. Amirkabir Journal of Mechanical Engineering. 48(4): 389-400. doi: 10.22060/mej.2016.522.

[47] Peckner, D. and Bernstein, I.M. 1977. Handbook of stainless steels.

[48] Soares, G.C., Rodrigues, M.C.M. and Santos, L.d.A. 2017. Influence of temperature on mechanical properties, fracture morphology and strain hardening behavior of a 304 stainless steel. Materials Research. 20(Suppl 2): 141-151. doi: 10.1590/1980-5373-MR-2016-0932.